

Nonlinear Refractory Plasmonics with Titanium Nitride Nanoantennas

Lili Gui,^{*,†} Shahin Bagheri,[†] Nikolai Strohfeldt,[†] Mario Hentschel,[†] Christine M. Zgrabik,[‡] Bernd Metzger,[†] Heiko Linnenbank,[†] Evelyn L. Hu,[‡] and Harald Giessen[†]

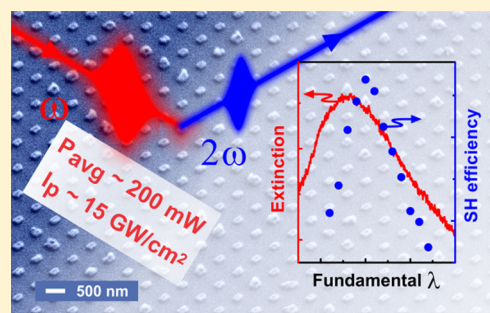
[†]4th Physics Institute and Research Center SCoPE, University of Stuttgart, Pfaffenwaldring 57, 70569 Stuttgart, Germany

[‡]School of Engineering and Applied Sciences, Harvard University, Cambridge, Massachusetts 02138, United States

S Supporting Information

ABSTRACT: Titanium nitride (TiN) is a novel refractory plasmonic material which can sustain high temperatures and exhibits large optical nonlinearities, potentially opening the door for high-power nonlinear plasmonic applications. We fabricate TiN nanoantenna arrays with plasmonic resonances tunable in the range of about 950–1050 nm by changing the antenna length. We present second-harmonic (SH) spectroscopy of TiN nanoantenna arrays, which is analyzed using a nonlinear oscillator model with a wavelength-dependent second-order response from the material itself. Furthermore, characterization of the robustness upon strong laser illumination confirms that the TiN antennas are able to endure laser irradiation with high peak intensity up to 15 GW/cm² without changing their optical properties and their physical appearance. They outperform gold antennas by one order of magnitude regarding laser power sustainability. Thus, TiN nanoantennas could serve as promising candidates for high-power/high-temperature applications such as coherent nonlinear converters and local heat sources on the nanoscale.

KEYWORDS: Nanooptics, refractory plasmonics, nonlinear optics, spectroscopy, second-harmonic generation, titanium nitride



Localized surface plasmon resonances can boost significantly the optical nonlinearity of metallic nanoparticles due to the strongly confined and enhanced electromagnetic near field.^{1–3} Efficient nonlinear optical processes such as second-^{4–19} and third-harmonic generation,^{20–29} four-wave mixing,^{30,31} optical parametric amplification,³² and so on from bare metallic nanostructures and hybrid nanosystems combining other highly nonlinear materials^{5,12,13,25,26,32,33} have been widely investigated, holding promise for a plethora of applications such as frequency conversion and ultrafast signal processing in integrated optics and nanophotonics,² all-optical near-field microscopy and spectroscopy,³⁴ chemical and biological sensing,^{6,35} etc. Among them, most of the plasmonic nanostructures are made of noble metals, for instance, gold. Such noble metal nanostructures benefit from high DC conductivity of the metals, and mature nanofabrication techniques, however, suffer from high loss in the optical and near-infrared (NIR) regions due to interband transitions occurring in the metals, poor processing compatibility with silicon fabrication standards, and importantly, structural and thermal instabilities upon intense confined local electric fields. These disadvantages limit to a large extent further exploration of metallic nanoparticles as efficient nonlinear sources at the nanoscale.

As a novel plasmonic material, titanium nitride (TiN) exhibits several promising properties. First, elaborate variation of the stoichiometry enables flexible tailoring of the optical

properties.³⁶ Second, high electron conductivity overcomes the loss obstacle for plasmonic applications. Furthermore, fabrication and integration advantages developed in CMOS technology allow for formation of ultrathin and ultrasoft layers with high quality and low loss.³⁷ It has been experimentally confirmed that TiN nanodisks show comparable linear plasmonic performances in the NIR region with respect to gold nanodisks.³⁸ Third, TiN is refractory with high melting point (>2900 °C), stable, and hard, possessing an outstanding thermal and chemical stability.³⁹ Fourth, recent investigations on the nonlinear optical responses from TiN thin films have already demonstrated fairly large second-⁴⁰ and third-order nonlinearities⁴¹ from the material itself, indicating the capability of TiN as a potential platform for high-power nonlinear plasmonics.

In this Letter we explore the nonlinear optical performance of TiN nanoantennas in the NIR range. Periodic TiN nanorod arrays are successfully fabricated which exhibit tunable plasmonic resonances from about 950 to 1050 nm by altering the antenna length. Second-harmonic spectroscopy is performed resonantly with respect to the plasmon resonances and can be theoretically described using a nonlinear oscillator

Received: June 10, 2016

Revised: August 1, 2016

Published: August 5, 2016

model when wavelength-dependent second-order susceptibility is taken into account. Based on a systematic comparison to gold nanorods with similar design parameters, the TiN nanoantennas exhibit excellent stability when exposed to intense incident laser irradiation with one order of magnitude stronger peak intensity and fluence than their gold counterparts, without degrading their optical properties and physical appearance. This is proven by measurement of second-harmonic-generation (SHG) intensity and the transmittance spectrum as well as scanning electron micrographs (SEMs). Although SHG intensity from the TiN antennas at the same excitation is still weaker than the gold antennas, dominated by worse linear plasmonic performances in terms of broader line width and smaller modulation depth of transmittance spectra, our TiN nanostructures enable generation of at least similarly large and steady SHG signals at much higher pump powers. In addition, in the spectral region of interest, the SHG signals from the TiN nanorods are purely coherent, excluding coexistence of two-photon photoluminescence (PL) and enabling an easier control of the functionalities as an integrated nonlinear nanodevice such as switching and modulation. Achievement of a clean, coherent, and efficient throughput of nonlinear optical signals upon strong pumping suggests that our TiN nanoantennas are very reliable and suitable for high-power nonlinear plasmonic applications.

The experimental setup for performing SH spectroscopy is schematically depicted in Figure 1a. A home-built laser source produces a transform-limited 30 fs Gaussian pulse train with average power of about 20 mW. It is employed as the fundamental light source, with flexible wavelength tunability in the range of about 900–1140 nm by means of a spatial light modulator in a 4f pulse shaper.^{23,42} The incident polarization is always along the rod long axis. The excitation laser is focused

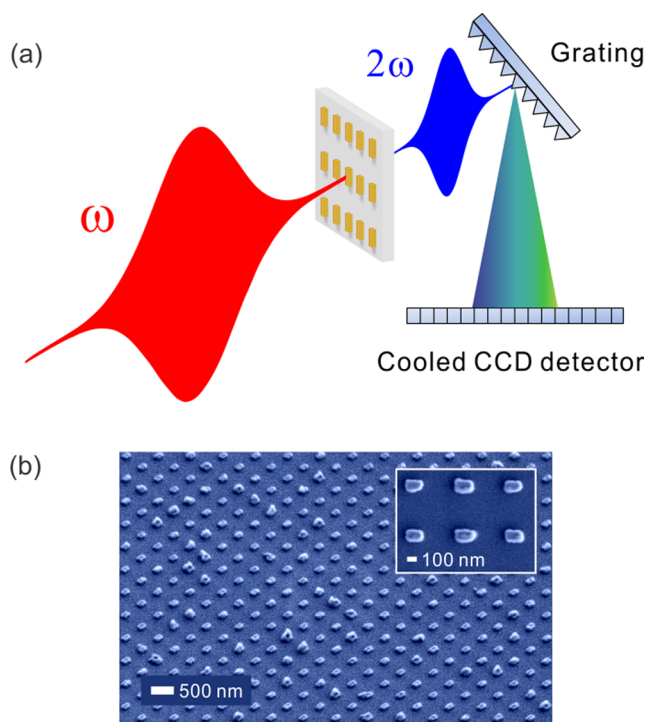


Figure 1. (a) Schematic setup of second-harmonic spectroscopy from TiN nanoantenna arrays. (b) Colored SEM images of the 180 nm long TiN antennas.

onto the sample with a spot size of about 50 μm . SHG signals from our TiN nanostructures are produced under normal incidence in transmission and then recorded by a cooled charge-coupled-device (CCD) camera attached to a spectrometer. We also measure SHG signals generated on the surface of a quartz crystal under oblique incidence (45°) in reflection for calibration of SH efficiencies at different wavelengths.⁴³ The following procedure describes the fabrication process of our TiN nanorods: First, homogeneous TiN layers with thickness of about 40 nm are deposited onto a sapphire substrate using nonreactive sputtering.^{44,45} Second, standard electron-beam lithography, development, evaporation of chromium, and subsequent lift-off are carried out to prepare chromium nanorods as an etch mask. After reactive-ion etching of our sample with Freon 12 (CCl_2F_2) and removal of the chromium nanostructures, periodic TiN nanorod arrays of $100 \times 100 \mu\text{m}^2$ are present on the sapphire substrate. In the process chromium with thickness of 40 nm is used as a mask to etch TiN enabling the etching selectivity ratio of about 100:1. The antenna width is approximately 100 nm, and the lattice constants in both directions are 500 nm. The antenna lengths for different fields are varied from about 180 to 210 nm in order to tailor the plasmon resonance frequencies within the spectral tuning window of our laser. Figure 1b shows colored SEM images of our TiN nanostructures with lengths of around 180 nm.

The linear plasmonic behavior of our TiN nanorods is characterized by transmittance T obtained at normal incidence with a white-light source linearly polarized along the antenna length. The red curves in Figure 2a depict the extinction [defined as $\alpha = -\ln(T)$] spectra for four different arrays with increasing rod lengths from 180 to 210 nm. The particle plasmon resonances are located within a range from about 950 to 1050 nm, respectively. For second-harmonic spectroscopy, we tune the center wavelength of the laser source from 920 to 1140 nm with a step size of 20 nm. For one fixed center wavelength, the SH spectrum of the TiN nanorods is fitted by a Gaussian function and then integrated over the wavelength, in order to obtain the overall SHG intensity at this particular center wavelength. After division by the SHG intensity from the quartz surface to eliminate spectral dependence of the entire setup when tuning the incident laser, wavelength-dependent SH efficiencies of the TiN nanostructures over the studied NIR region can be retrieved, as depicted by the blue dots in Figure 2a. Similar to previous research on third-harmonic generation (THG) of gold nanostructures in our group,^{22,23} the second-order nonlinear responses of TiN nanorods almost follow the extinction responses except for a slight red-shift of the peak SH efficiency with respect to the linear counterparts. The phenomenon of red-shifted peak can be understood by a harmonic oscillator model due to different responses between near field and far field caused by the damping term.⁴⁶ However, when we compare the nonlinear responses among different antenna arrays carefully, we find that the red-shift becomes less pronounced with longer antennas, implying that some other factor may play a role. Hence, we develop an extended nonlinear oscillator model in order to fully interpret the second-order responses from TiN antennas.

First, the localized surface plasmon is treated as a harmonic oscillator, which can then yield the extinction response²³

$$\alpha(\omega) = A \frac{\gamma \omega^2}{(\omega^2 - \omega_0^2)^2 + 4\gamma^2 \omega^2} \quad (1)$$

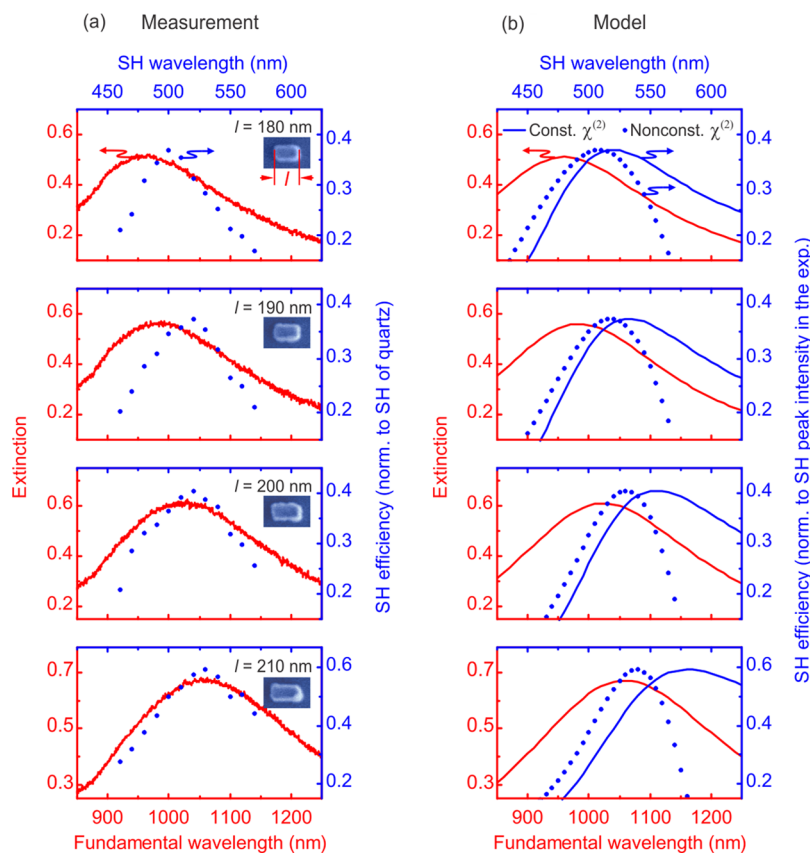


Figure 2. (a) Measured and (b) modeled normalized second-harmonic spectra (blue) of four TiN antenna arrays together with their extinction spectra (red). In the modeled SH spectra, for the blue solid curves a nonlinear oscillator model with ω -independent (constant) $\chi^{(2)}$ is considered, while for the blue dots the wavelength-dependent measured SH spectra of a TiN thin film normalized to SH of quartz (see Figure 3) are taken into account. The antenna lengths are increased from top to bottom from about 180 to 210 nm, as shown in the inset colored SEM images.

where γ denotes the damping parameter, ω_0 the plasmon resonance frequency, and A a scaling factor. All of the three parameters can be obtained when we fit eq 1 to the measured extinction spectra. The fitted extinction spectra are illustrated by the red curves in Figure 2b. The model gives very good agreement with the experiment for the linear plasmonic behavior. As for second-order optical response, an additional perturbation term has to be considered with the displacement, x , of the electrons in the form of

$$\ddot{x} + 2\gamma\dot{x} + \omega_0^2x + ax^2 = -\frac{e}{m}E(t) \quad (2)$$

where a describes the strength of SHG signal, e and m denote the charge and the effective mass of the electron, and $E(t)$ represents the external electric field, i.e., the 30 fs incident laser.

Based on perturbation theory, we can ultimately derive the second-harmonic term of x numerically, where a is chosen to match the peak value of the modeled result (see blue curves in Figure 2b) with that of the measurement. eq 2 with a constant a fails to elucidate the SH response well, especially when we compare the modeled results of the two longer antenna arrays with the measured ones. The reason is that we only take into account the influence from the plasmonic resonance, in which the second-order nonlinear susceptibility $\chi^{(2)}$ (equivalent to a) of the TiN material itself is nondispersive. Compared to the successful modeling of THG from gold nanostructures,^{22,23} the TiN nanoantennas here have worse plasmonic performances in terms of broader line width and smaller modulation depth of the extinction spectra, indicating that the maximum enhance-

ment factor of the local electric field near the resonance wavelength is neither significantly high nor dramatically distinct from that at another wavelength. In this case, the wavelength-dependent $\chi^{(2)}$ is of vital importance in the nonlinear model, as can be intuitively understood in the extreme situation where the resonant plasmonic effect vanishes in a nonstructured thin film.

In order to obtain the dispersive $\chi^{(2)}$, we perform SH spectroscopy of a TiN thin film in reflection at an angle of incidence of 45° , as indicated by the blue dots in Figure 3. The measured spectral dependence of SH efficiencies is fitted by a third-order polynomial and then interpolated; see the red curve in Figure 3. There are several important points that we would like to emphasize. First, a polynomial fit should be valid within a limited spectral range far away from any resonant bands such as interband transitions of TiN (less than 400 nm).^{36,41}

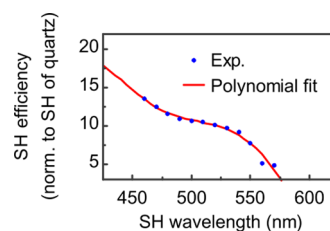


Figure 3. Measured (blue dots) and fitted (red curve) second-harmonic spectra of a TiN thin film normalized to that of a quartz surface.

Meanwhile, due to the interband transition at shorter wavelength than our SH range, it is easy to comprehend that the SHG signals increase toward shorter wavelength in the investigated spectral span.⁴⁷ Second, taking the SH efficiencies of a gold film with thickness of 100 nm which we measured before⁴⁷ as a reference, we infer that the TiN material itself indeed exhibits a similarly large second-order nonlinearity when compared with gold. After multiplying the aforementioned modeled results by the wavelength-dependent SH efficiencies of the TiN thin film, we can eventually model the SH spectra of TiN antennas (indicated by the blue dots in Figure 2b). The good agreement between measurement and our model confirms that a nonlinear oscillator which considers both the resonance effect and the nonlinear material dispersion is capable of unraveling the wavelength-dependent second-order response of our TiN nanorod arrays. As additional evidence, the nonlinear oscillator model excluding the material dispersion enables perfect prediction of the SH spectra of a TiN antenna array when normalized to those of a TiN thin film (see Figure S1).

To characterize the high power sustainability of our TiN nanorods upon laser exposure, we perform a series of SHG experiments with the 180 nm long antenna array by increasing pump power up to one order of magnitude stronger than those in Figure 2a, achieving the maximum peak and average power we can reach in our current laser system. To do so, a much broader and structured laser spectrum without amplitude shaping is employed; see Figure S2a. A typical SH spectrum from the nanorods is depicted in red in Figure S2b. An integrated SH intensity over the wavelength range of 450–570 nm is calculated, and its evolution upon gradually ramping up the pump power is represented by blue dots on a log–log scale in Figure 4a. Every data point takes 1 min of exposure time. The blue arrow indicates the measurement sequence. A strictly linear fit with slope around 2.0 (the red dashed line) over the whole power tuning region matches the SHG process as expected and also indicates good durability of the TiN nanostructures upon strong laser illumination (average power up to 200 mW at 44 MHz repetition rate, and peak intensity up to 15 GW/cm²). When we repeat the SHG experiments once again with gradually ramping down the pump power, the nonlinear intensities almost recover within a negligible measurement error (green circles in Figure 4a). The excellent robustness of the TiN nanoantennas is further confirmed by invariant transmittance spectra before and after intense irradiation of the 200 mW laser for half an hour, as displayed by red solid and blue dotted curves in Figure 4b, respectively. Moreover, the SEM images in Figure 4c demonstrate almost the same microscopic appearances of the antenna array at different areas (unexposed border area, red box; exposed central areas, blue boxes) after illumination with the 200 mW laser for 1 h. Benefiting from the refractory properties of TiN, the nanorods possess excellent thermal and optical stability upon strong laser exposure, verified by comprehensive nonlinear and linear optical characterization in addition to morphology.

In a stark contrast to TiN nanorods, gold nanorods fabricated on a sapphire substrate with a similar structural design and nearly the same resonance frequency respond quite differently to strong laser excitation. As depicted in Figure 4d, we carry out SH experiments for the gold nanorod array in a similar manner to the situation for the TiN array. A typical nonlinear spectrum of such a gold array is described by the blue

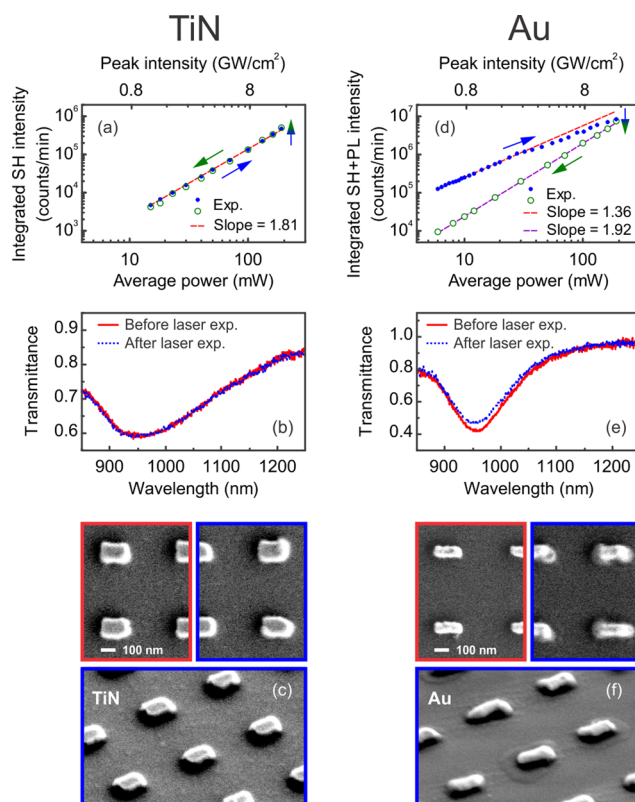


Figure 4. Characterization of robustness of (a–c) the 180 nm long TiN antenna array and (d–f) an Au antenna array with similar plasmon resonance frequency upon strong laser illumination. (a, d) Integrated intensity of second-harmonic generation (for Au, including photoluminescence) of the two arrays as a function of incident average power and peak intensity. Arrows indicate the measurement sequence, namely, first increasing power (blue dots), and then decreasing power (green circles). (b, e) Comparison of transmittance spectra before and after strong laser irradiation experiments. (c, f) SEM images of unexposed (red box) and exposed (blue boxes) areas of the two arrays after 200 mW strong laser irradiation for 60 min (TiN) and 30 min (Au), respectively. All SEM images have the same magnification.

curve in Figure S2b. Note that pronounced two-photon photoluminescence occurs, indicated by the strong emission beyond 570 nm, which stems from the onset of interband transition of gold near 500 nm.⁴⁸ Since the SHG and PL signals cannot be distinguished simply from the spectrum, we just calculate the overall nonlinear response by integrating the spectrum again within the span of 450–570 nm. The change of this response with rising excitation power is plotted by the blue dots in log–log scale in Figure 4d. A linear fit with a slope of 1.36, indicated by the red dashed line, does not stretch over the entire power range but is only valid at pumping on the order of average power of 10 mW. The weaker output than expected by the red line above 40 mW is a clear indication of optical damage of the gold antennas. Even the distinctly lower slope than 2.0 might hint toward slight optical damage at pump powers below 10 mW. Actually, a duplicate of such a gold antenna array was previously damaged at a power of about 10 mW, and the nonlinear emission intensity could no longer be achieved (not shown here). Indeed, after the series of increasing excitation power, when decreasing the power consecutively, the nonlinear response (green circles) is much weaker than the former values at the same power. The series of nonlinear measurements of decreasing power gives a linear slope of 1.92 (purple dashed),

more approaching the theoretical value of 2.0 than the increasing-power series, which we believe is a hint of different behavior of the gold antennas between scaling up and down the pump intensity. It is because that the gold nanostructures accumulated gradually optical damage and became more impaired with increasing power, while they were not damaged further in the decreasing-power series. The transmittance spectra before and after the measurements in Figure 4d are depicted in Figure 4e by red solid and blue dotted curves, respectively. It is easy to observe that the plasmon resonance is less pronounced, followed by a slight blue shift after laser irradiation, which can explain the weaker nonlinear intensities in the decreasing-power series than the increasing-power series in Figure 4d. The SEM images in Figure 4f provide more structural details to reveal change of the gold array after 200 mW laser exposure for half an hour. In contrast to the unexposed area displayed inside the red box, the exposed areas depicted inside blue boxes demonstrate melting features of the gold rods, particularly visible near the edges. Overall, the gold nanorod array can only withstand laser illumination with roughly one order of magnitude less power than the TiN array. The reason could be multifold: First, TiN has a much higher melting point with better structural and thermal stability than Au. Second, the TiN nanorods exhibit a wider and less pronounced plasmon resonance, indicating a weaker near-field enhancement than Au nanorods. Hence the local heat accumulation might be less than in the Au counterparts. However, the local heating efficiency from TiN nanostructures could be higher than Au nanostructures,³⁸ making the consideration of heat transfer more complicated. To answer this question unambiguously, a thermal analysis has to be carried out experimentally by a proper means, for instance, by a thermal camera, which is unfortunately not available in our setup at this moment. On the other hand, we notice that a direct heating experiment carried out by Li et al.⁴⁹ has clearly demonstrated much better robustness against deformation of TiN nanostructures compared to Au counterparts after annealing at 800 °C. Their TiN nanoparticles can endure laser irradiation of only less than 15.5 W/cm²,⁴⁹ weaker than our case with average power intensity of about 10⁴ W/cm². We attribute this discrepancy to different laser sources and different TiN structures.

It is very instructive to compare the SHG intensities between TiN and Au nanoantennas. Because of the pronounced presence of photoluminescence at the broadband incidence, it is difficult to give a quantitative comparison of SHG signals based on Figure 4a and d. Therefore, we again employ transform-limited 30 fs Gaussian pulses as the excitation source. In this situation we study the 210 nm long TiN nanorod array and another fresh gold nanorod array with a similar plasmon resonance frequency. The comparison of the SHG spectra generated by the fundamental laser of 1000 and 1060 nm center wavelength respectively indicates that the TiN nanoantennas emit 1–2 orders of magnitude lower SHG signals than the Au counterparts near the resonance wavelength at the same fundamental power (see Figure S3a and b), suffering from the poorer plasmonic performance of TiN nanorods and hence the lower quality factor.²² It is caused mainly by larger damping present in our fabricated TiN thin films, i.e., larger imaginary part of permittivity of TiN with respect to that of Au in the studied spectral region.⁵⁰ However, it is worth mentioning that the one order of magnitude higher laser power sustainability enables our TiN nanoantennas to act as a comparably efficient

SHG emitter at stronger fundamental power. With improved fabrication techniques, the dielectric function of TiN is expected to be optimized,^{36,44,50,51} so that a larger nonlinear response of TiN nanoparticles might be very likely in future.

In conclusion, we successfully fabricated periodic TiN nanorod arrays resonant in the vicinity of 1 μm and carried out systematic studies on second-harmonic spectroscopy and high-power laser durability. A nonlinear oscillator model, taking the dispersive material second-order responses into account, was developed to unravel the wavelength-dependent second-harmonic efficiencies. A detailed comparison between TiN nanorods and Au counterparts confirmed the unprecedented performance of TiN nanoparticles, including excellent robustness upon 1 order of magnitude stronger laser irradiation as well as fairly efficient and coherent nonlinear emission. Our finding opens new avenues for further exploration of TiN nanostructures in a broad range of applications such as nonlinear signal converters, biological and chemical sensing, photocatalysis, heat-assisted magnetic recording, and so forth.

■ ASSOCIATED CONTENT

📄 Supporting Information

The Supporting Information is available free of charge on the ACS Publications website at DOI: 10.1021/acs.nanolett.6b02376.

Equations S1 and S2, detailed derivations for explaining our nonlinear oscillator model. Figure S1, modeled extinction and SH spectra of the 210 nm TiN antenna array compared with the measured SH efficiencies normalized to those of a TiN thin film. Figure S2, typical spectra of excitation laser and nonlinear emission from TiN and Au nanorods for characterization of their high power sustainabilities. Figure S3, comparison of state of polarization and intensities of SHG at different excitation wavelengths between TiN and Au nanoantennas exhibiting similar plasmon resonance wavelength at about 1050 nm. Figure S4, measured transmitted SH spectra of a TiN thin film on a sapphire substrate and a bare sapphire substrate at orthogonally polarized normal incidences. Figure S5, experimentally measured and numerically calculated transmittance spectra of the TiN and the Au nanorods in Figure S3 with incident light polarized perpendicular to the rod length (PDF)

■ AUTHOR INFORMATION

Corresponding Author

*E-mail address: l.gui@pi4.uni-stuttgart.de.

Notes

The authors declare no competing financial interest.

■ ACKNOWLEDGMENTS

The authors gratefully acknowledge financial support from the Baden-Württemberg Stiftung (Kompetenznetz Funktionelle Nanostrukturen), from the DFG (SPP1391, Ultrafast Nanooptics), from the BMBF (13N10146), and the ERC (Complexplas). L.G. additionally acknowledges financial support by the Carl-Zeiss-Stiftung. This work was performed in part at the Harvard University Center for Nanoscale Systems (CNS), a member of the National Nanotechnology Coordinated Infrastructure Network (NNCI), which is supported by the National Science Foundation under NSF award No. 1541959. The

authors thank Dr. Marc Widenmeyer (Institute for Materials Science, University of Stuttgart) for X-ray diffraction measurements and Monika Ubl for technical assistance with the etching process.

REFERENCES

- (1) Schuller, J. A.; Barnard, E. S.; Cai, W.; Jun, Y. C.; White, J. S.; Brongersma, M. L. *Nat. Mater.* **2010**, *9*, 193–204.
- (2) Kauranen, M.; Zayats, A. V. *Nat. Photonics* **2012**, *6*, 737–748.
- (3) Chen, P.-Y.; Argyropoulos, C.; Alù, A. *Nanophotonics* **2012**, *1*, 221–233.
- (4) Butet, J.; Duboisset, J.; Bachelier, G.; Russier-Antoine, L.; Benichou, E.; Jonin, C.; Brevet, P.-F. *Nano Lett.* **2010**, *10*, 1717–1721.
- (5) Pu, Y.; Grange, R.; Hsieh, C.-L.; Psaltis, D. *Phys. Rev. Lett.* **2010**, *104*, 207402.
- (6) Ray, P. C. *Chem. Rev.* **2010**, *110*, 5332–5365.
- (7) Niesler, F. B.; Feth, N.; Linden, S.; Wegener, M. *Opt. Lett.* **2011**, *36*, 1533–1535.
- (8) Aouani, H.; Navarro-Cia, M.; Rahmani, M.; Sidiropoulos, T. P.; Hong, M.; Oulton, R. F.; Maier, S. A. *Nano Lett.* **2012**, *12*, 4997–5002.
- (9) Linden, S.; Niesler, F.; Förstner, J.; Grynko, Y.; Meier, T.; Wegener, M. *Phys. Rev. Lett.* **2012**, *109*, 15502.
- (10) Thyagarajan, K.; Butet, J. r. m.; Martin, O. J. *Nano Lett.* **2013**, *13*, 1847–1851.
- (11) Czaplicki, R.; Husu, H.; Siikonen, R.; Mäkitalo, J.; Kauranen, M.; Laukkanen, J.; Lehtolahti, J.; Kuittinen, M. *Phys. Rev. Lett.* **2013**, *110*, 093902.
- (12) Lehr, D.; Reinhold, J. r.; Thiele, I.; Hartung, H.; Dietrich, K.; Menzel, C.; Pertsch, T.; Kley, E.-B.; Tünnermann, A. *Nano Lett.* **2015**, *15*, 1025–1030.
- (13) Grinblat, G.; Rahmani, M.; Cortés, E.; Caldarola, M.; Comedi, D.; Maier, S. A.; Bragas, A. V. *Nano Lett.* **2014**, *14*, 6660–6665.
- (14) Accanto, N.; Piatkowski, L.; Renger, J.; van Hulst, N. F. *Nano Lett.* **2014**, *14*, 4078–4082.
- (15) Lee, J.; Tymchenko, M.; Argyropoulos, C.; Chen, P. Y.; Lu, F.; Demmerle, F.; Boehm, G.; Amann, M. C.; Alu, A.; Belkin, M. A. *Nature* **2014**, *511*, 65–69.
- (16) O'Brien, K.; Suchowski, H.; Rho, J.; Salandrino, A.; Kante, B.; Yin, X.; Zhang, X. *Nat. Mater.* **2015**, *14*, 379–383.
- (17) Celebrano, M.; Wu, X.; Baselli, M.; Großmann, S.; Biagioni, P.; Locatelli, A.; De Angelis, C.; Cerullo, G.; Osellame, R.; Hecht, B. *Nat. Nanotechnol.* **2015**, *10*, 412–417.
- (18) Black, L.-J.; Wiecha, P. R.; Wang, Y.; de Groot, C. H.; Paillard, V.; Girard, C.; Muskens, O. L.; Arbouet, A. *ACS Photonics* **2015**, *2*, 1592–1601.
- (19) Dong, Z.; Asbahi, M.; Lin, J.; Zhu, D.; Wang, Y. M.; Hippalgaonkar, K.; Chu, H.-S.; Goh, W. P.; Wang, F.; Huang, Z.; Yang, J. K. W. *Nano Lett.* **2015**, *15*, 5976–5981.
- (20) Hanke, T.; Krauss, G.; Trüttelein, D.; Wild, B.; Bratschitsch, R.; Leitenstorfer, A. *Phys. Rev. Lett.* **2009**, *103*, 257404.
- (21) Hanke, T.; Cesar, J.; Knittel, V.; Trügler, A.; Hohenester, U.; Leitenstorfer, A.; Bratschitsch, R. *Nano Lett.* **2012**, *12*, 992–996.
- (22) Hentschel, M.; Utikal, T.; Giessen, H.; Lippitz, M. *Nano Lett.* **2012**, *12*, 3778–3782.
- (23) Metzger, B.; Hentschel, M.; Lippitz, M.; Giessen, H. *Opt. Lett.* **2012**, *37*, 4741–4743.
- (24) Metzger, B.; Schumacher, T.; Hentschel, M.; Lippitz, M.; Giessen, H. *ACS Photonics* **2014**, *1*, 471–476.
- (25) Metzger, B.; Hentschel, M.; Schumacher, T.; Lippitz, M.; Ye, X.; Murray, C.; Knabe, B.; Buse, K.; Giessen, H. *Nano Lett.* **2014**, *14*, 2867–2872.
- (26) Aouani, H.; Rahmani, M.; Navarro-Cia, M.; Maier, S. A. *Nat. Nanotechnol.* **2014**, *9*, 290–294.
- (27) Chen, S.; Li, G.; Zeuner, F.; Wong, W. H.; Pun, E. Y. B.; Zentgraf, T.; Cheah, K. W.; Zhang, S. *Phys. Rev. Lett.* **2014**, *113*, 033901.
- (28) Wolf, D.; Schumacher, T.; Lippitz, M. *Nat. Commun.* **2016**, *7*, 10361.
- (29) Li, G.; Chen, S.; Pholchai, N.; Reineke, B.; Wong, P. W. H.; Pun, E. Y. B.; Cheah, K. W.; Zentgraf, T.; Zhang, S. *Nat. Mater.* **2015**, *14*, 607–612.
- (30) Danckwerts, M.; Novotny, L. *Phys. Rev. Lett.* **2007**, *98*, 026104.
- (31) Harutyunyan, H.; Volpe, G.; Quidant, R.; Novotny, L. *Phys. Rev. Lett.* **2012**, *108*, 217403.
- (32) Zhang, Y.; Manjavacas, A.; Hogan, N. J.; Zhou, L.; Ayala-Orozco, C.; Dong, L.; Day, J. K.; Nordlander, P.; Halas, N. J. *Nano Lett.* **2016**, *16*, 3373–3378.
- (33) Linnenbank, H.; Grynko, Y.; Förstner, J.; Linden, S. *Light: Sci. Appl.* **2016**, *5*, e16013.
- (34) Kravtsov, V.; Ulbricht, R.; Atkin, J. M.; Raschke, M. B. *Nat. Nanotechnol.* **2016**, *11*, 459–464.
- (35) Mesch, M.; Metzger, B.; Hentschel, M.; Giessen, H. *Nano Lett.* **2016**, *16*, 3155–3159.
- (36) Patsalas, P.; Kalfagiannis, N.; Kassavetis, S. *Materials* **2015**, *8*, 3128–3154.
- (37) Naik, G. V.; Shalaev, V. M.; Boltasseva, A. *Adv. Mater.* **2013**, *25*, 3264–3294.
- (38) Guler, U.; Ndukaife, J. C.; Naik, G. V.; Nnanna, A. G. A.; Kildishev, A. V.; Shalaev, V. M.; Boltasseva, A. *Nano Lett.* **2013**, *13*, 6078–6083.
- (39) Guler, U.; Boltasseva, A.; Shalaev, V. M. *Science* **2014**, *344*, 263–264.
- (40) Capretti, A.; Wang, Y.; Engheta, N.; Dal Negro, L. *ACS Photonics* **2015**, *2*, 1584–1591.
- (41) Kinsey, N.; Syed, A. A.; Courtwright, D.; DeVault, C.; Bonner, C. E.; Gavrilenko, V. I.; Shalaev, V. M.; Hagan, D. J.; Van Stryland, E. W.; Boltasseva, A. *Opt. Mater. Express* **2015**, *5*, 2395–2403.
- (42) Metzger, B.; Steinmann, A.; Giessen, H. *Opt. Express* **2011**, *19*, 24354–24360.
- (43) Metzger, B.; Gui, L.; Fuchs, J.; Floess, D.; Hentschel, M.; Giessen, H. *Nano Lett.* **2015**, *15*, 3917–3922.
- (44) Zgrabik, C. M.; Hu, E. L. *Opt. Mater. Express* **2015**, *5*, 2786–2797.
- (45) Bagheri, S.; Zgrabik, C. M.; Gissibl, T.; Tittel, A.; Sterl, F.; Walter, R.; De Zuani, S.; Berrier, A.; Stauden, T.; Richter, G.; Hu, E. L.; Giessen, H. *Opt. Mater. Express* **2015**, *5*, 2625–2633.
- (46) Zuloaga, J.; Nordlander, P. *Nano Lett.* **2011**, *11*, 1280–1283.
- (47) Metzger, B.; Gui, L.; Giessen, H. *Opt. Lett.* **2014**, *39*, 5293–5296.
- (48) Olmon, R. L.; Slovick, B.; Johnson, T. W.; Shelton, D.; Oh, S.-H.; Boreman, G. D.; Raschke, M. B. *Phys. Rev. B: Condens. Matter Phys.* **2012**, *86*, 235147.
- (49) Li, W.; Guler, U.; Kinsey, N.; Naik, G. V.; Boltasseva, A.; Guan, J.; Shalaev, V. M.; Kildishev, A. V. *Adv. Mater.* **2014**, *26*, 7959–7965.
- (50) Naik, G. V.; Schroeder, J. L.; Ni, X.; Kildishev, A. V.; Sands, T. D.; Boltasseva, A. *Opt. Mater. Express* **2012**, *2*, 478–489.
- (51) Yang, Z.-Y.; Chen, Y.-H.; Liao, B.-H.; Chen, K.-P. *Opt. Mater. Express* **2016**, *6*, 540–551.